Journal of Alloys and Compounds 786 (2019) 139–148

Contents lists available at ScienceDirect

Journal of Alloys and Compounds

journal homepage: http://www.elsevier.com/locate/jalcom

Structure formation and mechanical properties of the high-entropy AlCuNiFeCr alloy prepared by mechanical alloying and spark plasma sintering

A.I. Yurkova [a], V.V. Cherniavsky [a], V. Bolbut [b], M. Krüger [b, c], I. Bogomol [a, *]

[a] National Technical University of Ukraine "Igor Sikorsky Kyiv Polytechnic Institute", 37 Peremohy Ave., Kyiv, 03056, Ukraine
[b] Institute of Materials and Joining Technology, Otto-von-Guericke University Magdeburg, Universitätsplatz 2, 39106, Magdeburg, Germany
[c] Institute of Energy and Climate Research, IEK-2, Research Center Jülich, Germany

ARTICLE INFO

Article history:
Received 10 September 2018
Received in revised form
17 January 2019
Accepted 28 January 2019

Keywords:
High-entropy alloy
Mechanical alloying
Spark plasma sintering
Mechanical properties
Thermal analysis

ABSTRACT

The phase and structural transformations in equiatomic powder compositions of the Al-Cu-Ni-Fe-Cr system during mechanical alloying (MA), annealing and subsequent spark plasma sintering (SPS) had been studied by X-ray diffraction analysis, scanning and transmission electron microscopy, and differential scanning calorimetry. It has been established that the nanocrystalline high-entropy AlCuNiFeCr alloy synthesized during MA consists of a supersaturated solid solution with a bcc crystalline structure. After annealing and spark plasma sintering at 800 °C, the alloy becomes three-phased, and consists mainly of one B2-ordered solid solution, one fcc solid solution (25 wt %), and of the $(Cr, Fe)_{23}C_6$ phase (8 wt %). The Vickers hardness of the sintered AlCuNiFeCr alloy was 8.35 GPa, and the compressive strength at room temperature reached 1960 MPa.

1. Introduction

Usually, traditional industrial metal alloys consist of one main solvent element with a small number of several alloying additives, which enhance their operational properties [1–4]. Under certain conditions, such alloys become thermodynamically unstable. When high temperatures are applied, phase transformations may occur which can lead to the deterioration of operational properties. In many cases, an excessive amount of alloying elements leads to the formation of intermetallic compounds which modify the properties in terms of increased strength, and decreased ductility of the alloys [2].

The industrial development of many industries requires new structural and tool materials with improved operational properties, which are able to work under high temperatures, intensive wear and dynamic mechanical loads. Improving the working capacity of such materials is an urgent and important task. One of the most promising classes of materials is high-entropy alloys (HEAs) [5]. They are based on a new concept of chemical compositions in metal alloys. According to this concept, the high entropy of mixing of various metal elements with a concentration close to equiatomic, can significantly reduce the Gibb's free energy of mixing, and stabilize solid solutions with a relatively simple crystal structure and a good combination of properties [1,6–12].

The creation of such materials and their application in science and technology requires the systematic study of the conditions, mechanisms for the formation of the structure and phase composition, as well as ways to find how to implement their potential characteristics [13].

The HEAs can be prepared by the same methods as traditional alloys: various ingot metallurgical technologies, powder metallurgical routes, which may include mechanical alloying (MA), water atomization, deposition of films and coatings, etc. [1,6,7,14–17]. Every method has its advantages and disadvantages. In comparison with other methods, MA enables the formation of a microstructure with a homogeneous chemical composition [18]. The formation of homogeneous solid solutions at ambient temperature is the main advantage of MA over casting, especially in the case of multicomponent alloys with large differences in the melting temperatures of the initial components. Moreover, MA allows to form the fine-grained or even nanocrystalline structures, which typically improves the mechanical properties (Hall-Petch hardening) of

* Corresponding author.
E-mail address: ubohomol@iff.kpi.ua (I. Bogomol).

https://doi.org/10.1016/j.jallcom.2019.01.341
0925-8388/

these alloys in contrast to other methods mentioned above [9,14,15]. However, the information about the elements dissolution as well as the sequence of the stages of phase evolution during MA and sintering are limited, and requires a more detailed study [2]. Therefore, the purpose of this work was to study the processes of formation of the phase composition, the grain structure, and the mechanical properties of the AlCuNiFeCr HEA prepared by MA, and consolidated by spark plasma sintering (SPS).

2. Experimental procedure

2.1. Preparation of the material

The metallic powders of Al, Cu, Ni, Fe, Cr with 99.8% purity, for each element, and particle size of ≤45 μm in equal molar fractions (20 at. %) were used as starting material.

According to Refs. [19–21], the resultant structure of HEAs is determined by these three factors: a high entropy of mixing ($\Delta Smix > 13{,}38\ J\ K^{-1} \bullet mol^{-1}$), which is the dominant factor; a slight difference in the atomic radii of components ($\delta < 8.5\%$ - responsible for the formation of a crystalline structure rather than amorphous and $\delta \leq 4\%$ - responsible for the formation of a solid solutions rather than intermetallic compound); and an enthalpy of mixing ($-10\ kJ\ mol^{-1} < \Delta Hmix < 5\ kJ\ mol^{-1}$). According to the calculations which were carried out in accordance with [1,11,22], it had been found that for the selected alloy components of the Al-Cu-Ni-Fe-Cr system, the entropy of mixing is $\Delta Smix = 1.61 \cdot R = 13.38\ J\ K^{-1}\ mol^{-1}$, the difference in atomic radii is $\delta = 5.62\%$, and the enthalpy of mixing is $\Delta Hmix = -4.0\ kJ\ mol^{-1}$.

Due to above mentioned parameters we can conclude that the AlCuNiFeCr HEA could contain intermetallic compounds.

Mechanical alloying of the metallic powders mixture was carried out in a planetary mill with a rotational speed of 580 rpm. The weight of the powders mixture was taken proportionately to the weight of milling bodies in a ratio of 1:10. The chambers and milling bodies with a 10 mm diameter, produced from hardened ShH-15 steel (in analogy to 52100 steel (USA)), were used in the experiment. To prevent the oxidation and excessive cold welding of the powders, both within the chamber and the milling bodies, as well as among the powders themselves causing agglomeration, the milling process was carried out in a gasoline medium.

To reduce the porosity and to increase the density as well as to preserve the nanocrystalline state for optimum mechanical properties of the alloy, the consolidation of the MA powders was carried out by the SPS method (FCT HP D 25) at a pressure of 150 MPa, and at temperatures of 700, 800 and 900 °C with a dwell time of 15 min (except for one trial of 5 min at 800 °C).

2.2. Material characterization

The shape, size and microstructure of the powder particles as well as the microstructure of the consolidated alloys were studied using a scanning electron microscope (SEM) REMMA-101A, and a transmission electron microscope (TEM) JEM-CX. For the microstructure observation, the samples were sequentially polished, and then etched with active oxide polishing suspension solutions. The chemical composition of the alloy was determined using energy-dispersive X-ray (EDX) microanalysis in a SEM equipped with an energy-dispersive detector.

Phase distribution, the structure of the Al-Cu-Ni-Fe-Cr powder mixture at various stages of the MA process and the AlCuNiFeCr alloy after the SPS were investigated using an X-ray diffractometer Rigaku Ultima IV (Japan) in monochromatic Cu-K_α radiation. A graphite single crystal mounted on a diffracted beam was used as a monochromator. The X-ray diffractograms were obtained for 2θ angles in the 20–120° range. The scanning step was 0.04° with an angular speed of the goniometer rotation of 2°/min.

The average size of crystallites in powder alloys was determined by the broadening of diffraction profiles according to the generally accepted method [14] excluding the influence of instrumental expansion. The lattice parameters of solid solutions were calculated according to the positions of the gravitation centers of the diffraction profiles at large angles based on the Wulff–Bragg's condition [23].

The thermal stability of the AlCuNiFeCr HEA powder structure was studied using differential scanning calorimetry (DSC) STA449F1 (NETZSCH, Germany). Thermal effects during heating from 30 °C to 1430 °C were recorded and compared with the weight change of samples. The heating rate was 20 °C/min. The DSC method was carried out by the simultaneous heating of two calorimetric cells (working and standard) in a constant stream of high-purity Argon at a rate of 40 ml/min. Measurement and data processing were carried out in accordance with the method described in Ref. [24].

The Vickers hardness of the alloys was determined at a load of 1.5 N on the MHV 1000 (Time Group Inc., China) device.

The compressive strength of the sintered AlCuNiFeCr alloy was carried out using rectangular samples with a cross section of 2 × 2 mm, and a height of 3.5 mm, which were prepared by electro-discharge machining and grinding. The samples were tested using a Zwick/Roell Z100 electromechanical testing machine equipped with a Maytec furnace at temperatures of 20, 400, 600, and 800 °C at a loading speed of 0.5 mm/min.

3. Results and discussion

3.1. Microstructure and phase formation of CuNiAlFeCr HEA during MA

The transformations of the equiatomic Al-Cu-Ni-Fe-Cr powder mixture at various stages of the mechanical alloying process are shown in Fig. 1. The initial X-ray diffraction spectrum of the powder mixture is a superposition of the diffraction peaks for the initial pure components. After 0.5 h of MA, the peak intensity for all components decreases significantly, while the width increases. At the same time, the Al peaks almost disappear from the X-ray diffraction spectrum (Fig. 1), and only 4 of the 5 components (Cu, Ni, Fe and Cr) are observed in the microstructure of the powder

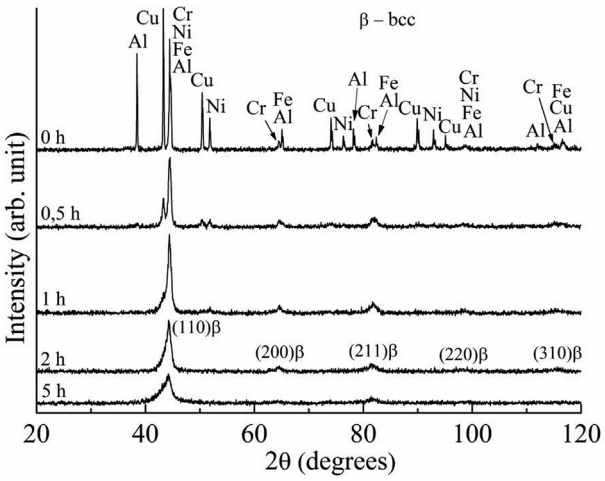

Fig. 1. X-ray diffraction spectra of the equiatomic Al-Cu-Ni-Fe-Cr powder mixture at various stages of MA in a planetary mill in gasoline media.

particles (Fig. 2 a), which may be due to the solid solution formation.

Even at the initial stage of MA (0.5 h), the diffraction peaks for Cu, Ni, Fe and Cr have a strong tailing, and a low intensity, which makes them very difficult to detect at high diffraction angles (Fig. 1). The significant tailing of the diffraction peaks, and a decrease in their intensity indicate a significant fragmentation of the crystallites, and a high level of internal micro-stresses [14,25–28].

After 1 h of MA, only a very weak Ni peak (at an angle of $2\theta \approx 51^{\circ}$) is observed in the X-ray diffraction spectrum (Fig. 1), whereas the peaks for Cu and Al disappear almost completely. The complete merging of the Fe and Cr diffraction peaks indicates the beginning of the formation of a bcc solid solution (β-phase). The parameter of the bcc solid solution lattice after 1 h of MA is a = 0.2889 nm. At the same time, the microstructure of the MA powder particles (Fig. 2 b) becomes finer compared to the powder particles after 0.5 h of MA (Fig. 2 a).

With the increase of MA duration to 2 h, only peaks for the bcc solid solution (β-phase) are observed in the X-ray diffraction spectrum (Fig. 1). When their intensity decreases and the width increases, it indicates a distortion of the lattice due to the mixing of different sized elements in a common lattice, an increase of internal micro-stresses, and a subsequent refinement of the structure [29]. At the same time, the shift of the peaks to smaller diffraction angles is observed, which corresponds to an increase in the lattice parameter of the bcc solid solution (β-phase) (a = 0.2894 nm). The increase in the lattice parameter of the bcc solid solution (Fig. 3) could be explained by an intense dissolution of Al atoms, which has the largest atomic radius among all components of the AlCuNiFeCr HEA [30,31]. The microstructure of the particles becomes homogeneous and inhomogeneities of elemental distribution in the powder particles are not observed in the SEM micrographs (Fig. 2 c).

By increasing the milling time to 5 h, no significant changes in the X-ray diffraction spectrum (Fig. 1) are observed. The phase composition of the AlCuNiFeCr HEA remains unchanged, and only the most intense reflexes of the bcc lattice are visible in the spectrum, which indicates the completion of structure formation of the solid solution. A decrease in height and a greater tailing of the peaks are typical features for a nanocrystalline structure formation. As well as a high level of micro-stresses (crystal lattice distortions) which is the result of intensive plastic deformation during MA and mixing of different sized elements in a common lattice of solid solution [14,27,29,32].

The homogenized microstructure after 5 h of treatment in a planetary mill (Fig. 2 d) confirms the above findings from the XRD analyses, and the completion of the alloying process [14].

The completion of the alloying process is also confirmed by the results of a chemical analysis (Table 1). It is shown that the concentration deviation of the components does not exceed 2 at. % of the initial chemical composition in different parts of the particle, and within different powder particles. After 5 h of MA, the lattice parameter of the bcc solid solution (β-phase) became a = 0.2893 nm, and the particle size distribution ranged from 1 to 50 μm with an average value of 14 μm (Fig. 4).

The alloying process starts when the density of the defects in the material as well as the contact area between the components are substantially increased due to the refining of the grain structure to nanostructural dimensions [33,34]. The alloy formation in the Al-Cu-Ni-Fe-Cr system started in the time interval from 0.5 to 1 h, which correlates with the time necessary to achieve the nanostructural state in this system [33,34]. The average crystallite size was near 60 nm after 1 h of MA, and it decreased to about 17 nm (Fig. 5) when processed for 5 h in a planetary mill. These results

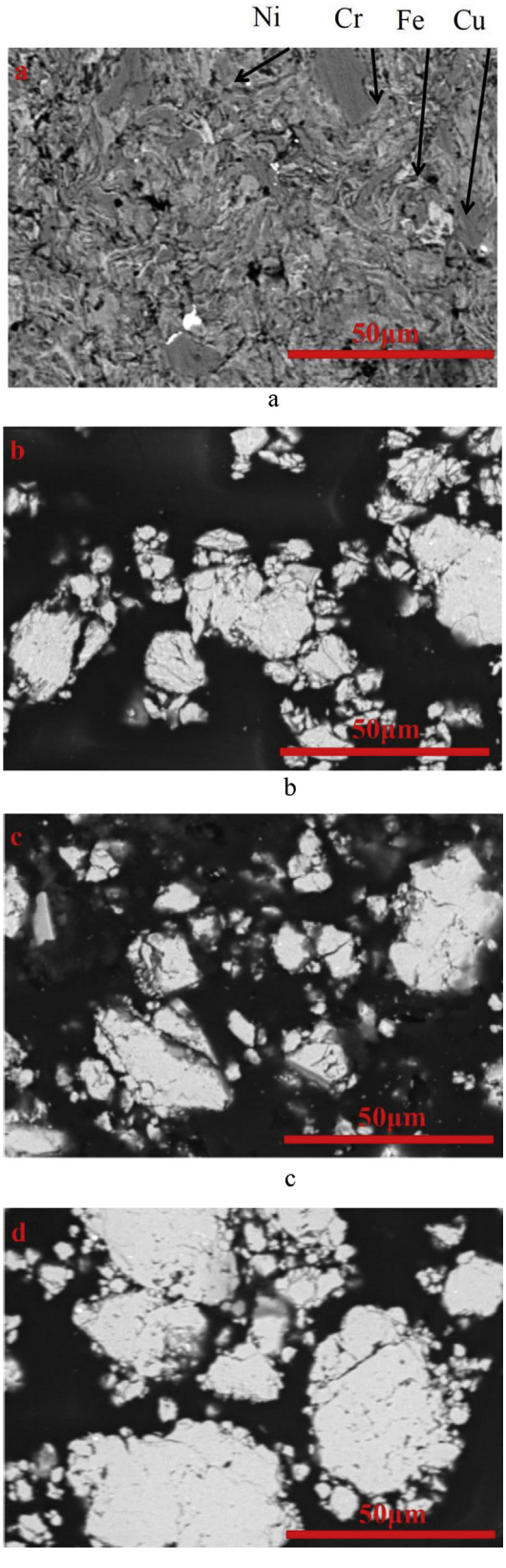

Fig. 2. SEM images of the microstructure of the HEA AlCuNiFeCr powder at different stages of MA in planetary mill in gasoline media: a) 0.5 h; b) 1 h; c) 2 h; d) 5 h.

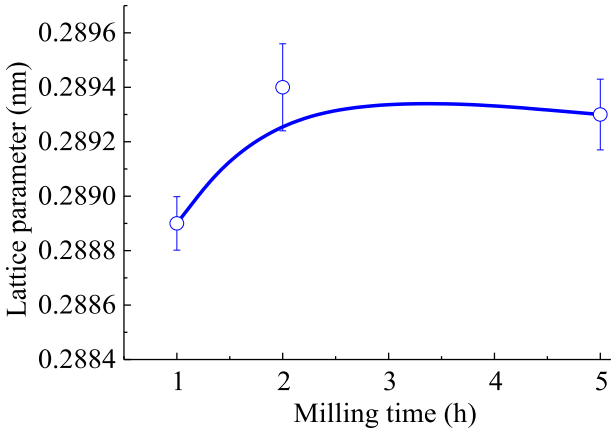

Fig. 3. Change in the lattice parameter of the bcc solid solution in the AlCuNiFeCr alloy during MA in a gasoline medium.

Table 1
Chemical composition of AlCuNiFeCr HEA powder after 5 h of MA in planetary mill in a gasoline medium.

Chemical element	Initial chemical composition, at. %	Chemical composition after MA, at. %
Al	20	18.05
Cr	20	22.03
Fe	20	19.61
Ni	20	18.94
Cu	20	21.37

were obtained by estimations, which were based on X-ray diffraction analysis as well as on the TEM analysis (Fig. 6). The crystallite sizes found by both methods correlate well with each other (Figs. 5 and 6).

The difference in atomic radii between all components (except of Al) for the investigated AlCuNiFeCr HEA is small (Table 2). Therefore, the most of the atoms can be easily interchanged, and have the same ability to occupy sites in the crystalline lattice to form the solid solution especially in conditions of the non-equilibrium MA process [31–36]. Moreover, the high entropy of mixing for a 5-component alloy ($\Delta S_{mix} = 13.38\ J\ K^{-1} \bullet mol^{-1}$) reduces the tendency of ordering and segregation, facilitates

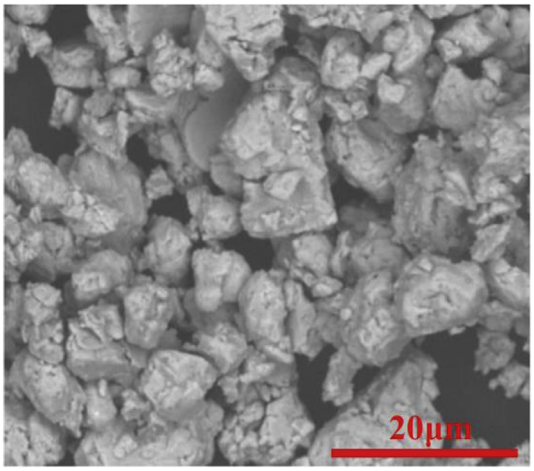

Fig. 4. Particle morphology of the AlCuNiFeCr alloy after 5 h of MA.

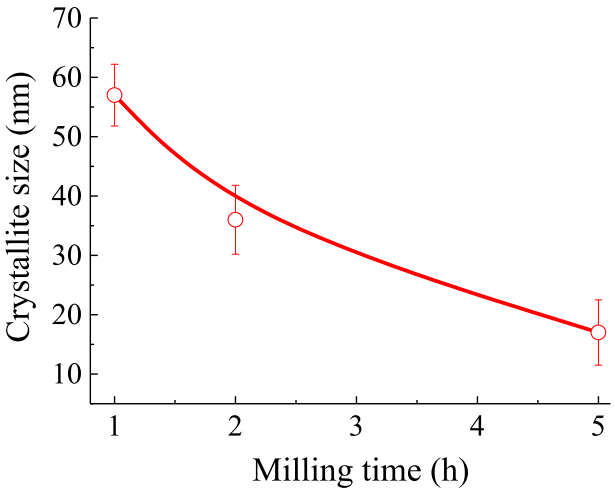

Fig. 5. Changes in the crystallite size in the AlCuNiFeCr alloy during the MA in planetary mill in a gasoline medium.

formation of solid solutions, and increases their stability when compared with intermetallics [11]. An increase of solubility of components in a solid state is also due to the non-equilibrium state, which was formed during the MA process, and leads to formation of supersaturated solid solutions. As described above, mechanical alloying occurs when the size of the crystallites decreases to the nanostructural level. Thus, due to the large volume fraction of grain boundaries in nanocrystalline alloys, the considerable amount of energy (enthalpy) is accumulated which serves as a driving force for the formation of the solid solution. The increase of this energy leads to the increased solubility in the solid state [32,37,38].

It is shown that the bcc solid solution is formed in the investigated HEA although Al, Cu and Ni are fcc metals (Fig. 5). This phenomenon could be explained by the fact that Al is a bcc stabilizer at concentrations more than 15% due to the formation of directed *p-d* hybrid orbitals with transition metals [20,39]. Because of the high atomic radius of Al between atoms in the AlCuNiFeCr alloy (Table 2), it is difficult for Al to be embedded in a denser fcc lattice, which leads to the formation of a more open bcc structure. The latter has a fill factor of 0.68 compared to the more densely packed fcc lattice which has a fill factor of 0.72. Consequently, the bcc lattice provides the dissolution of other elements without significant lattice expansion and distortion compared to the fcc.

Also, it was found that the dissolution of the alloy components directly depends on the physical properties of the elements. Table 2

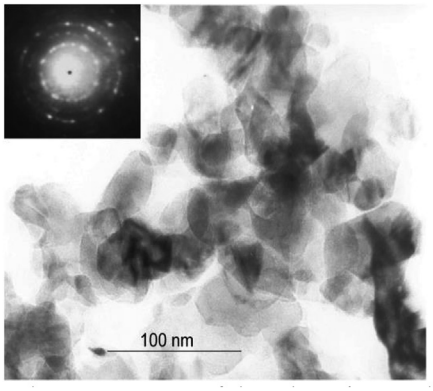

Fig. 6. TEM brightfield image and SAED pattern of the AlCuNiFeCr alloy powder structure after 5 h of MA in a gasoline medium.

Table 2
Characteristics of elements of the alloy [21,23].

Element	Atomic radius, nm	Crystal structure (400 K)	Melting point, °C	Self-diffusion coefficient (400 K)
Al	0.143	fcc	660	10^{-19}
Fe	0.127	bcc	1538	10^{-31}
Cu	0.128	fcc	1083	10^{-27}
Cr	0.130	bcc	1857	10^{-41}
Ni	0.125	fcc	1453	10^{-37}

shows the main properties of the elements included in the AlCuNiFeCr alloy, which are the most influential factors [38,40]. The crystal structure and diffusion properties are given for a temperature of 400 K (127 °C) because this is the typical MA temperature measured during the process [33]. According to the diffusion theory, it is well known that in traditional alloy systems there is a strong dependency between the diffusion coefficient and the melting point T_m [30,36]. This means that a metal with a higher T_m has an increased bonding strength, and therefore a lower self-diffusion coefficient compared to an element with a lower T_m. Thus, elements with a lower melting point could diffuse more easily into a crystal lattice than an element with a higher T_m [30]. Although this empirical ratio is based on the diffusion of different types of atoms in the same matrix from the main element. The obtained X-ray diffraction data (Fig. 1) show that the above-mentioned temperature dependency on the diffusion coefficient could also be extended to the self-diffusion of elements in the multicomponent matrix [36]. This means that there is a simple correlation between the alloying/dissolution sequence and the melting point (Table 2).

In accordance with the data of X-ray analyses, the point of view of kinetics and the temperature dependency on the diffusion coefficients, it appears that the dissolution of the components during the formation of alloys within the Al-Cu-Ni-Fe-Cr system may occur in the following order: Al → Cu → Ni → Fe → Cr.

3.2. Thermal stability of AlCuNiFeCr HEA

Fig. 7 shows the results of differential scanning calorimetry of the AlCuNiFeCr alloy prepared by MA in a gasoline medium for 5 h. The interpretation of the DSC data was carried out taking into account the results of the X-ray phase analysis of samples following annealing at different temperatures (Fig. 8).

During the first heating, the endothermic peak at 72 °C on the DSC curve was observed, which is associated with the evaporation of the adsorbed substances. The wide exothermic effect occurring from 100 to 520 °C is related to the reorganization of the dislocation structure, the relaxation of internal micro-stresses acquired during MA, and the increase of the crystallite size, which is confirmed by the results of the X-ray diffraction analysis of the annealed specimens (Fig. 8) and data [41–43].

The next exothermic effect starting at 551°C indicates the dissipation of energy during phase transformation (separation of the α-phase). The horizontal playground appearing at 671°C remains at a temperature of 800°C, and indicates the growth of crystallites. The next extended endothermic region on the DSC curve indicates a gradual destruction of the crystalline structure at high temperatures up to the melting of the alloy's three phases: two solid solutions and the $(Fe,Cr)_{23}C_6$ phase, as evidenced by three exothermic peaks, which appear at 1162°C, 1229°C, and 1310 °C, respectively. A similar behavior was also observed in Refs. [41–44]. After the reheating of the sample, the exothermic peaks were not observed, that indicates the thermodynamic stability of the phase composition of the multicomponent alloy.

The X-ray diffraction spectra of the AlCuNiFeCr powder milled for 5 h, and annealed for 1 h at various temperatures, are shown in Fig. 8. After annealing at 500 °C, the initial bcc solid solution is transformed into an B2-ordered solid solution. As a result, a new peak at $2\theta = 31.06°$ was observed. In addition to the peaks for the B2-ordered solid solution, peaks for the fcc solid solution (α-phase)

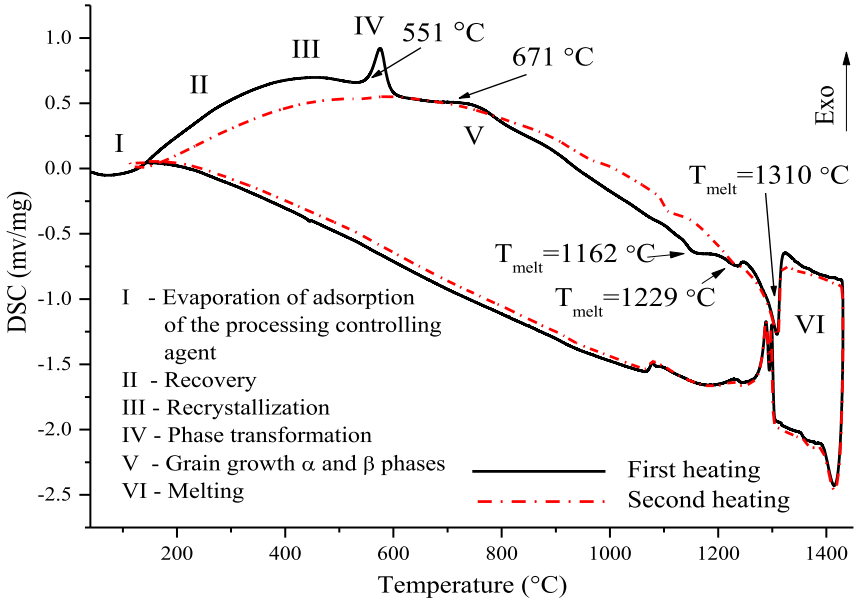

Fig. 7. DSC curves of the AlCuNiFeCr powder prepared by MA in a gasoline medium.

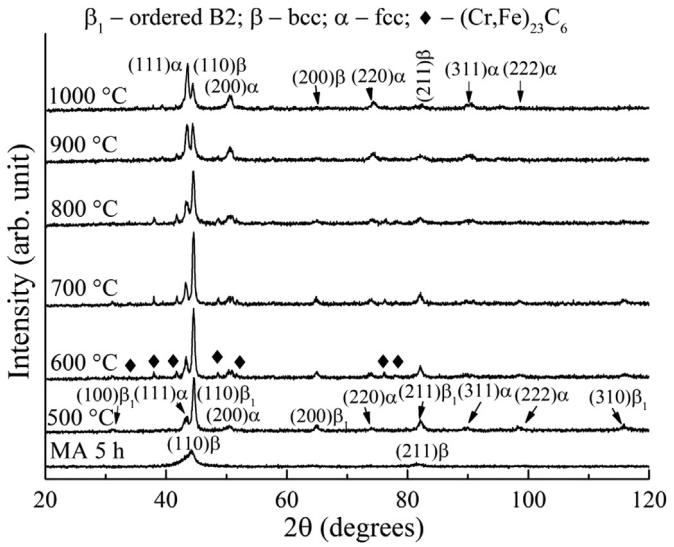

Fig. 8. X-ray diffraction spectra of the MA AlCuNiFeCr alloy powder after annealing at different temperatures for 1 h.

were also found in the X-ray diffraction spectrum (Fig. 8). Consequently, the alloy becomes two-phased. Moreover, the shift in the diffraction peaks for the B2-ordered solid solution to larger 2θ angles is observed, that indicates a decrease in the period of the crystal lattice (Table 3), which is related to the release of the α-phase, and the redistribution of elements between the α- and ordered B2 solid solution. The decrease in the width of the diffraction lines for the ordered B2 solid solution, and the increase in their intensity, indicate the decrease in the defect density for the crystal lattice. As well as the increase in the average size of crystallites due to the processes of returning and recrystallization, that fully corresponds to the DSC data (Fig. 7). Similar behavior had been also described in Ref. [43] for the CoCrFeNiAl alloy prepared by MA.

The appearance of the diffraction peaks for the fcc phase is related to the decomposition of the metastable supersaturated bcc solid solution, and confirmed by the DSC data (Fig. 7) – the presence of the exothermic peak at 551 °C. Due to the higher dwell time during annealing (1 h) compared with DSC (heating rate of 20°/min), the phase transformation of bcc → ordered B2 solid solution + fcc was probably carried out at lower temperatures.

After annealing at 600°C, the $(Fe,Cr)_{23}C_6$ phase as well as the α-phase and the ordered B2 solid solution are observed (Fig. 8). The $(Fe,Cr)_{23}C_6$ phase could have been formed during heat treatment as a result of the reaction of the metals with gasoline. It could be adsorbed in the closed pores formed during MA.

The increase of the annealing temperature to 700°C does not lead to different results in the phase compositions as compared to the annealing at 600 °C. Annealing at 800, 900 and 1000 °C resulted in an increase in the fcc solid solution (α-phase) content as indicated by the increased intensity of the corresponding interference peaks. At the same time, the intensity of the peaks of the B2-ordered solid solution is decreased. After annealing at 900°C, the intensity of the diffraction lines for the $(Fe,Cr)_{23}C_6$ phase is significantly decreased; after annealing at 1000°C, the diffraction lines almost completely disappear from the X-ray diffraction spectrum (the content of the $(Fe,Cr)_{23}C_6$ phase is about 2 wt%). Also, the interference peak at the angle $2\theta \approx 31^\circ$ (100) that belongs to the B2-ordered solid solution, disappeared after annealing at 900 and 1000°C, instead, an B2 phase was formed. This can happen by the redistribution of elements between α- and B2-ordered solid solution. A similar effect of the phase transformation of the supersaturated bcc solid solution into a phase with ordered B2 and fcc crystal structures was described in Refs. [41,42].

The phase transformations occurring at elevated temperatures are associated with the metastable state of the supersaturated solid solution formed under conditions of intense plastic deformation during MA. This solid solution is transformed into more thermodynamically stable B2-ordered and fcc solid solutions during annealing. However, according to the diffraction pattern (Fig. 8), the structure of the alloy remained nanocrystalline. In the temperature range from 700°C to 900°C, the interference peaks are shifted: the ordered B2 solid solution shifts to smaller angles, and the α-phase (fcc) to larger angles indicating a change in the lattice parameter (Table 3). Obviously, this fact is linked to the redistribution of components, especially aluminum, which has the largest atomic radius in the Al-Cu-Ni-Fe-Cr system (Table 2).

3.3. Phase composition and microstructure of SPSed AlCuNiFeCr HEA

In order to determine the optimal temperature-time modes of

Table 3
Changing of the phase composition and crystal lattice period of the AlCuNiFeCr HEA prepared by MA in a gasoline medium after isothermal annealing for 1 h at different temperatures.

Annealing temperature, °C	Phase composition, weight %			Crystal lattice period *a*, нм	
	fcc	$(Fe,Cr)_{23}C_6$	ordered B2	fcc	ordered B2
500	21	0	79	0.3618	0.2899
600	22	7	71	0.3626	0.2895
700	21	8	71	0.3615	0.2887
800	25	10	65	0.3616	0.2894
900	46	7	47	0.3613	0.2903
1000	61	2	37	0.3609	0.2899

Table 4
Sintering modes and properties of the AlCuNiFeCr alloy.

Sintering temperature, °C	Dwell time, min	Porosity, %	Phase distribution, weight %		
			ordered B2	fcc	$(Fe,Cr)_{23}C_6$
700	15	5.4	61	29	10
800	5	1.1	63	29	9
800	15	0.6	67	25	8
900	15	0.6	64	27	9

treatment by SPS of the powders obtained by MA, a study on the influence of time and temperature on the sintering process was conducted. The experiment were carried out in the temperature range of 700–900 °C with dwell times from 5 to 15 min (Table 4).

The microstructure is strongly affected by the sintering temperature and dwell times (Fig. 9). The AlCuNiFeCr sample sintered at 700 °C for 15 min, shows dense regions, the residual porosity of the sample being 5.4% (Fig. 9 a, Table 4).

Using XRD analysis, it was found that the bcc supersaturated solid solution prepared during MA was decomposed into three additional equilibrium phases during SPS at 700 °C: an ordered B2 solid solution, a fcc crystal structures and a $(Fe,Cr)_{23}C_6$ phase (Fig. 10), to which correspond the gray, the light gray, and the dark gray phases, respectively, in Fig. 9a. The phase distribution is shown in Table 4.

Increasing the sintering temperature to 800 °C leads to a decrease in the porosity to 0.6% (Fig. 9 b). Strong bonds were formed between the former particles boundaries. The phase distribution is the same as for the samples sintered at 700°C (Fig. 10, Table 4). As shown in Fig. 9 a and b, the SPSed AlCuNiFeCr HEA exhibits three distinctive regions (Region 1 - light-gray, 2 – gray, and 3 - dark-gray) representing a three-phased microstructure identified by XRD. Moreover, we found that the dark-gray phase (Region 3) of the SPSed AlCuNiFeCr HEA could be easily removed by an active oxide polishing suspension solution. An investigation of the chemical composition of the phases by EDS shows that all phases contain all the components of the alloy (Table 5). The light-gray phase has high concentration of Cu and Ni (more than Al, Fe, Cr). The gray phase has high concentrations of Al, Fe and Cr, and the dark-gray phase has high concentrations of Fe and Cr.

Based on the XRD pattern (Fig. 10), the ordered B2 solid solution is the main phase in the AlCuNiFeCr HEA. Probably, this phase is based on elements, which have a bcc structure (like Fe and Cr) or Al, and stabilizes the bcc phase in the HEA [7,39]. Since the gray phase is dominant in these samples (Fig. 9 a, b), and is enriched by Al, Fe and Cr, it could correspond to the ordered B2 solid solution. The light-gray phase corresponds to the fcc phase because it is based on the Cu and Ni elements, which also have a fcc structure. According to the XRD and SEM analyzes, the $(Fe,Cr)_{23}C_6$ phase corresponds to the quantity of the dark-gray areas in the structure that is enriched by the Fe and Cr elements (Fig. 9 b, Table 5).

For the two light-gray and gray phases (fcc and ordered B2), the valence electrons concentration (VEC) was calculated taking into account their chemical composition (Table 5). The VEC for the light-gray and gray areas are 10.5 and 6.6 electrons/atom, respectively, which should contribute to the formation of the bcc and fcc crystal structures in these phases [20,45].

Increasing the sintering temperature to 900 °C does not result in a change of the alloy's density (Table 4), but the size of the gray and light gray phases are noticeably increased (Fig. 9 c). The phase distribution of the alloy is almost unchanged in comparison to SPSed samples at 700 and 800 °C (Table 4) as also shown by the XRD analysis (Fig. 10). Thus, the optimal sintering temperature for the AlCuNiFeCr alloy is 800 °C.

In order to determine the optimum dwell time for the SPS, another experiment was performed with an exposure time of 5 min at a temperature of 800 °C. The porosity of the samples was 1.1% (Fig. 9 d, Table 4) which is quite high when compared to 0.6% for the alloy sintered at the same temperature with a dwell time of 15 min. The phase distribution and the microstructure are almost identical for the samples SPSed at 800 °C with a dwell time of 15 min as confirmed by the XRD spectra (Fig. 10, Table 4). The formation of ordered B2 and fcc solid solutions correlates with the conditions for the formation of phase composition in the HEAs, and is determined by the VEC value [20,45].

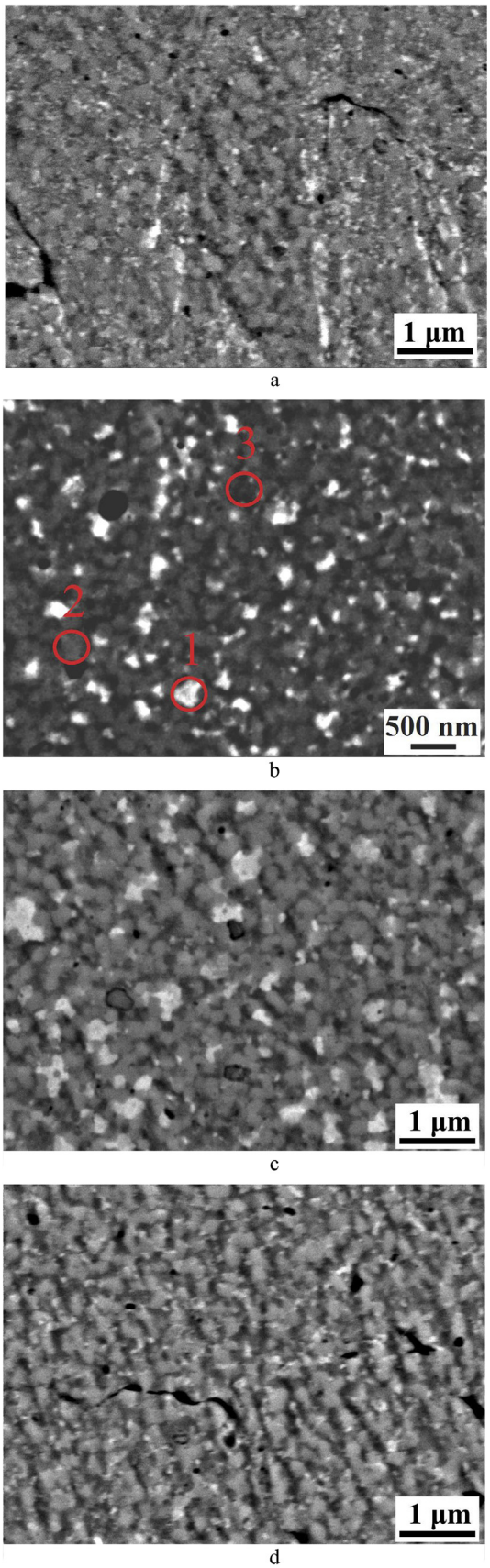

Fig. 9. Microstructure of the AlCuNiFeCr alloy SPSed at different temperatures and dwell times: a) 700°C, 15 min; b) 800°C, 15 min; c) 900 °C, 15 min; d) 800° C, 5 min.

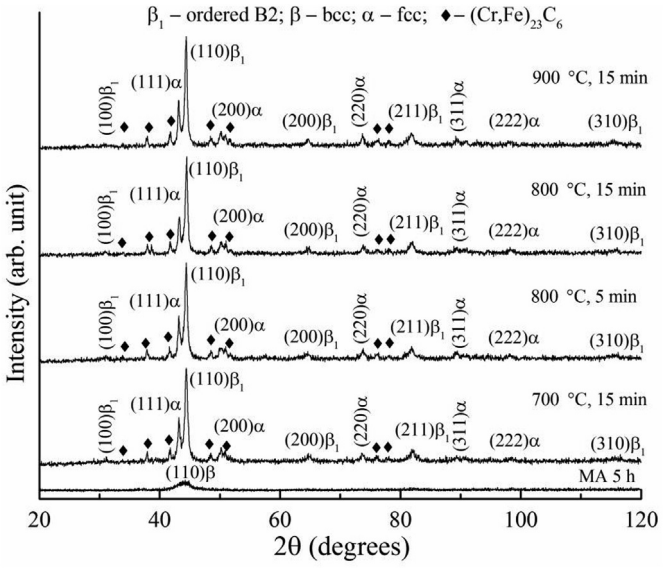

Fig. 10. XRD spectrum of the AlCuNiFeCr alloy SPSed at different modes.

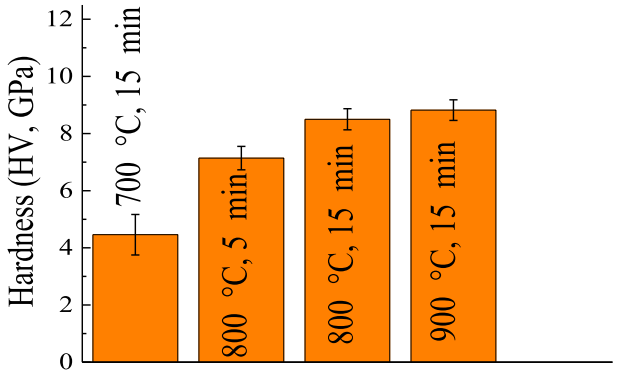

Fig. 11. Vickers hardness of the SPSed AlCuNiFeCr alloy.

3.4. Mechanical properties of SPSed AlCuNiFeCr HEA

The Vickers hardness values of the AlCuNiFeCr alloy sintered at different modes are shown in Fig. 11. The highest hardness is observed for samples sintered at 800 °C and 900 °C for 15 min. However, the difference between the values lies in the measurement error range. Thus, the optimal mode for preparing the AlCuNiFeCr HEA consists in a sintering temperature of 800 °C ($\approx 0.6T_{melt}$), and a dwell time of 15 min. Such a mode allows to achieve minimum porosity, and an increased uniformity in the distribution of the components, and of the fcc phase in the alloy.

The stress-strain curves of the AlCuNiFeCr HEA sintered at 800 °C for 15 min obtained at room and elevated temperatures, are shown in Fig. 12. The highest compression strength of 1960 MPa is observed for samples tested at room temperature. Increasing the testing temperature to 400 °C leads to an increase in plasticity, and a slight decrease in the strength to 1800 MPa. Further increases in the testing temperature to 600 and 800 °C causes a drop in the strength down to 490 and 110 MPa, respectively. The yield strength of the AlCuNiFeCr alloy reached 1511 MPa at room temperature. An increase in temperature to 400 °C leads to decreasing the yield stress to 1366 MPa. At the temperature of 600 and 800 °C yield strength are decreased to 410 MPa and 48 MPa, respectively. The main reason for the increase in plasticity and decrease in strength is the high content of Cu-rich fcc phases in the alloy (Tables 4 and 5). The compression strength, yield strength values and Vickers hardness of the AlCuNiFeCr HEA at room temperatures are much higher than for CoCrFeNiV, CoCrFeNiMnV and $Al_{1.25}$CoCrCuFeNi alloys (compression strength of 1665, 1846 and 1820 MPa, yield strength of 1435, 1660 and 1480 MPa, HV of 5.87, 6.36, 4.9 GPa, respectively) [46,47].

The high strength of presented HEA is generated by the concurrent effect of several strengthening phenomena. The presence of hard particles of $(Fe,Cr)_{23}C_6$ carbides causes a significant increase in the compression strength and hardness of the AlCuNiFeCr HEA. The particle reinforcement effect had been also observed in Refs. [15,48–50]. The extremely reduced average grain size of the HEA, inherited from the severely plastically deformed MA powders, have caused obvious effect of grain boundary strengthening [48,51]. Moreover, the ordered B2 solid solution exhibits a lower plasticity than the fcc phase at room and elevated temperatures [31]. These effects cause notable decrease of plasticity up to 2.5% at room temperature (Fig. 12). Also, some contribution to strength values at room temperature is added by the effect of Al with its larger atomic radius compared to the other components, which can contribute to an improved effect of solid solution strengthening of the alloy [39,52,53].

The temperature dependence of the specific strength (SS) of the studied alloy is shown in Fig. 13. The SS values of two other high-entropy cast alloys, a ductile $Al_{0.5}$CoCrCuFeNi [19], a high-strength refractory TaNbHfZrTi [54] and a Ni-based superalloys, Inconel 718 [55,56] are given in this figure for comparison. The SS of the AlCuNiFeCr alloy is about 120 MPa/(g/cm^3) higher than the SS of the $Al_{0.5}$CoCrCuFeNi alloy at room temperature and at 400 °C. However, the AlCuNiFeCr alloy has a rapid drop of the SS in the temperature range of 400–600 °C. The SS of the AlCuNiFeCr alloy is the lowest between all presented alloys at a temperature of 800 °C. A possible reason for this could be due to a much lower melting temperature of Cu-rich fcc phase in the alloy [57,58]. A rapid decrease in strength in the alloys is known to generally occur at temperatures above T_r ~0.5–0.6 T_m due to intensification of diffusion-related processes [59,60].

4. Conclusion

The nanocrystalline equiatomic AlCuNiFeCr high-entropy alloy had been synthesized by mechanical alloying resulting in a supersaturated solid solution with a bcc crystal structure. The alloying process started when the structure was refined to a nanocrystalline

Table 5
Chemical composition and valence electrons concentration (VEC) of the AlCuNiFeCr alloy SPSed at 800 °C.

Alloy	Region	Concentration, at.%					VEC, electrons/atom
		Al	Cu	Ni	Fe	Cr	
AlCuNiFeCr	Alloy	19.44	19.38	19.82	21.62	19.74	7.6
	1	2.33	80.92	9.99	4.69	2.07	10.5
	2	25.97	8.12	11.31	28.05	26.55	6.6
	3	18.74	5.87	8.67	27.33	39.39	–

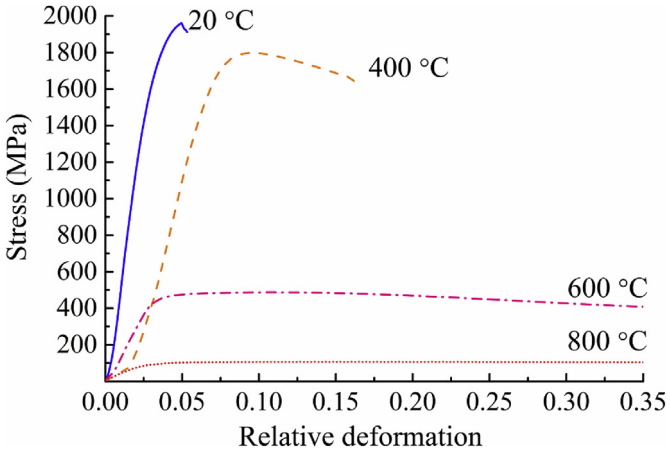

Fig. 12. Compressive stress-strain curves for the AlCuNiFeCr alloy tested at different temperatures.

state (less than 60 nm), whereas during the MA process the complete mutual solubility of the components was achieved. The mechanical alloying process allows shifting the boundaries for the formation of substitutional solid solutions beyond the limits typical for the equilibrium state.

The sequence of dissolution of the initial components during MA correlates with their melting temperature, and the formation of the substitutional solid solutions is carried out based on elements with low diffusion activity, that confirms the diffusion nature of the phase formation during mechanical alloying.

It is shown that by heating, the mechanically alloyed AlCuNiFeCr HEA decomposes from the metastable supersaturated bcc solid solution into the more stable phases with ordered B2 and fcc structures, that remained in the nanocrystalline size. Also the $(Fe,Cr)_{23}C_6$ phase is appeared in the AlCuNiFeCr HEA during heat treatment as a result of chemical reaction with gasoline residue, which was adsorbed in the closed pores formed during MA. The bulk AlCuNiFeCr HEA was prepared by spark plasma sintering. The microstructure of the composite represents the matrix with a structure of the B2-ordered solid solution, and dispersed inclusions of the fcc solid solution and $(Fe,Cr)_{23}C_6$ phase. The Vickers hardness of the samples was found in the 8.35–8.51 GPa range. The compressive strength of the SPSed AlCuNiFeCr HEA at room temperature reaches 1960 MPa, and decreases to 110 MPa with a testing temperature of 800 °C.

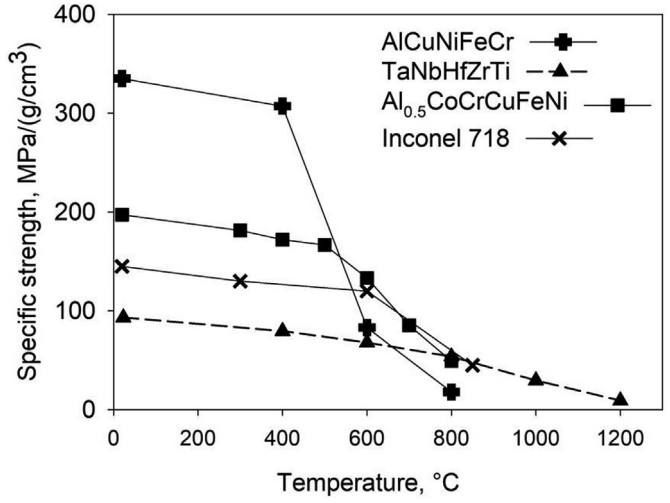

Fig. 13. The temperature dependence of the specific strength of the AlCuNiFeCr alloy in comparison with the $Al_{0.5}$CoCrCuFeNi, TaNbHfZrTi and Inconel 718 cast alloys.

Acknowledgements

The authors of this article acknowledge support received from the 0109U001776, 0115U000405, and 0116U006097 projects (Igor Sikorsky KPI, Ukraine). The authors also thank Dr. I. Solodkyi for his assistance in the preparation of the SPSed samples.

References

[1] J.-W. Yeh, S.-K. Chen, S.-J. Lin, J.-Y. Gan, T.-S. Chin, T.-T. Shun, C.-H. Tsau, S.-Y. Chang, Nanostructured high-entropy alloys with multiple principal elements; novel alloy design concepts and outcomes, J. Adv. Eng. Mater. 6 (2004) 299–303.
[2] F. Salemia, M.H. Abbasi, F. Karimzadeh, Synthesis and thermodynamic analysis of nanostructured CuNiCoZnAl high entropy alloy produced by mechanical alloying, J. Alloys Compd. 685 (2016) 278–286.
[3] E. Jumaev, S.H. Hong, J.T. Kim, H.J. Park, Y.S. Kim, S.C. Mun, K.B. Kim, Chemical evolution-induced strengthening on AlCoCrNi dual-phase high-entropy alloy with high specific strength, J. Alloys Compd. 777 (2018) 828–834.
[4] D.B. Miracle, O.N. Senkov, A critical review of high entropy alloys and related concepts, Acta Mater. 122 (2017) 448–511.
[5] W. Huoa, H. Zhoua, F. Fanga, X. Zhoua, Z. Xieb, J. Jianga, Microstructure and properties of novel CoCrFeNiTax eutectic high-entropy Alloys, J. Alloys Compd. 735 (2018) 897–904.
[6] C.-C. Yang, J.L.H. Chau, C.-J. Weng, C.-S. Chen, Y.-H. Chou, Preparation of high-entropy AlCoCrCuFeNiSi alloy powders by gas atomization process, J. Mater. Chem. Phys. 202 (2017) 151–158.
[7] R.X. Li, P.K. Liaw, Y. Zhang, Synthesis of Al_xCoCrFeNi high-entropy alloys by high-gravity combustion from oxides, Mater. Sci. Eng., A 707 (2017) 668–673.
[8] K. Yalamanchili, F. Wang, I.C. Schramm, J.M. Andersson, M.P. Johansson, Jöesaar F. Tasnádi, F. Mücklich, N. hafoor, M. Odén, Exploring the high entropy alloy concept in (AlTiVNbCr)N, J. Thin Solid Films 636 (2017) 346–352.
[9] J.-W. Yeh, S.-K. Chen, J.-Y. Gan, S.-J. Lin, T.-S. Chin, T.-T. Shun, C.-H. Tsau, S.-Y. Chang, Formation of simple crystal structures in Cu-Co-Ni-Cr-Al-Fe-Ti-V alloys with multiprincipal metallic elements, J. Metall. Mater. Trans. 35A (2004) 2533–2536.
[10] P.-K. Huang, J.-W. Yeh, T.-T. Shun, S.-K. Chen, Multi-Principal-element alloys with improved oxidation and wear resistance for thermal spray coating, J. Adv. Eng. Mater. 6 (2004) 74–78.
[11] J.-W. Yeh, Recent progress in high-entropy alloys, J. Ann. Chim. Sci. Mat. 31 (2006) 633–648.
[12] Y. Zhang, Y.J. Zhou, J.P. Lin, G.L. Chen, P.K. Liaw, Solid-solution phase formation rules for multi-component alloys, J. Adv. Eng. Mater. 10 (2008) 534–538.
[13] R. Sriharitha, B.S. Murty, R.S. Kottada, Alloying, thermal stability and strengthening in spark plasma sintered AlxCoCrCuFeNi high entropy alloys, J. Alloys Compd. 583 (2014) 419–426.
[14] S. Varalakshmi, M. Kamaraj, B.S. Murty, Formation and stability of equiatomic and nonequiatomic nanocrystalline CuNiCoZnAlTi high-entropy alloys by mechanical alloying, Metall. Mater. Trans. A 41 (2010) 2703–2709.
[15] I. Moravcika, J. Cizekb, Z. Kovacovac, J. Nejezchlebovad, M. Kitzmantelc, E. Neubauerc, I. Kubenae, V. Hornike, I. Dlouhy, Mechanical and microstructural characterization of powder metallurgy CoCrNi medium entropy alloy, Mater. Sci. Eng. A 701 (2017) 370–380.
[16] C.-C. Yang, J.L. Hang, C.-J. Weng, C.-S. Chen, Y.-H. Chou, Preparation of high-entropy AlCoCrCuFeNiSi alloy powders by gas atomization process, Mater. Chem. Phys. 202 (2017) 151–158.
[17] D. Yim, M.J. Jang, J.W. Bae, J. Moon, C.-H. Lee, S.-J. Hong, H.S. Kim, Compaction behavior of water-atomized CoCrFeMnNi high-entropy alloy powders, Mater. Chem. Phys. 210 (2018) 95–102.
[18] Y.-L. Chena, C.-W. Tsaib, C.-C. Juanb, M.-H. Chuangb, J.-W. Yehb, T.-S. Chinc, S.-K. Chend, Amorphization of equimolar alloys with HCP elements during mechanical alloying, J. Alloys Compd. 506 (2010) 210–215.
[19] C.-W. Tsaia, M.-H. Tsaia, J.-W. Yeh, C.-C. Yang, Effect of temperature on mechanical properties of Al0.5CoCrCuFeNi wrought alloy, J. Alloys Compd. 490 (2010) 160–165.
[20] S. Guo, C.T. Liu, Phase stability in high entropy alloys: formation of solid-solution phase or amorphous phase, Prog. Mater. Sci.: Met. Mater. Int. 21 (2011) 433–446.
[21] M.-x. Ren, B.-s. Li, H.-z. Fu, Formation condition of solid solution type high-entropy alloy, Trans. Nonferrous Metals Soc. China 23 (2013) 991–995.
[22] A.L. Greer, Thermodynamics of solids, Nature 336 (1993) 303–304. Nonferrous Met. Soc. China, 23 (2013), 991–995.
[23] Y.S. Umansky, Y.A. Skakov, A.N. Ivanov, L.N. Rastorguev, Crystallography, X-ray and electron microscopy. - M .: Metallurgy, 1994, 632 p.
[24] A.K. Jena, A.K. Gupta, M.C. Chaturvedi, A differential scanning calorimetric investigation of precipitation kinetics in the Al-1.53 wt% Cu-0.79 wt% Mg alloy, Acta Metall. 37 (1989) 885–889.

[25] N.I. Noskova, R.R. Mulyukov, Submicrocrystalline and Nanocrystalline Metals and Alloys, UrO RAN, Ekaterinburg, 2003.
[26] M.R. Fitzsimmons, J.A. Eastman, M. Muller-Stach, G. Wallner, Structural characterization of nanometer-sized crystalline Pd by X-ray –diffraction techniques, Phys. Rev. B 44 (1991) 2452–2460.
[27] X. Zhu, R. Beringer, U.A. Herr, H. Gleiter, X-ray diffraction studies of the structure of nanometer-sized crystalline materials, Phys. Rev. B 35 (1987) 9085–9090.
[28] I.V. Aleksandrov, R.Z. Valiev, Investigation of nanocrystalline materials using X-ray diffraction analysis, Phys. Metals Metal Sci. 77 (1994) 77–87.
[29] Y.F. Ye, Y.H. Zhang, Q.F. He, Y. Zhuang, S. Wang, S.Q. Shi, Y. Yang, Atomic-scale distorted lattice in chemically disordered equimolar complex alloys, Acta Mater. 150 (2018) 182–194.
[30] D.A. Porter, K. E Easterling, Phase Transformations in Metals And Alloys, Chapman & Hall, London, 1992.
[31] C. Kittel, Introduction to Solid State Physics, John Wiley & Sons, New York, 1996.
[32] C. Suryanarayana, Mechanical alloying and milling, Prog. Mater. Sci. 46 (2001) 1–184.
[33] L. Lu, M.O. Lai, Formation of new materials in the solid state by mechanical alloying, Mater. Des. 16 (1995) 33–39.
[34] L. Lu, M. Lai, S. Zang, Diffusion in mechanical alloying, J. Mater. Process. Technol. 67 (1997) 100–104.
[35] Y. Zhang, Y.J. Zhou, J.P. Lin, G.L. Chen, P.K. Liaw, Solid-solution phase formation rules for multi-component alloys, Adv. Eng. Mater. 10 (2008) 534–538.
[36] J.-W. Yeh, S.-K. Chen, J.-Y. Gan, S.-J. Lin, T.-S. Chin, T.-T. Shun, C.-H. Tsau, S.-Y. Chang, Formation of simple crystal structures in Cu-Co-Ni-Cr-Al-Fe-Ti-V alloys with multiprincipal metallic elements, Metall. Mater. Trans. A 35A (2004) 2533–2536.
[37] H.X. Sui, M. Zhu, M. Qi, G.B. Li, D.Z. Yang, The enhancement of solid solubility limits of AlCo intermetallic compound by high-energy ball milling, J. Appl. Phys. 71 (1992) 2945–2949.
[38] F.R. de Boer, R. Boom, W.C.M. Mattens, A.R. Miedema, A.K. Niessen, Cohesion in Metals: Transition Metal Alloys, Elsevier, New York, 1988.
[39] X. Yang, Y. Zhang, P.K. Liaw, Microstructure and compressive properties of NbTiVTaAlx high entropy alloys, J. Procedia Eng. 36 (2012) 292–298.
[40] A. Takeuchi, A. Inoue, Calculation of mixing enthalpy and mismatch entropy for ternary amorphous alloys, Mater. Trans., JIM 41 (2000) 1372–1378.
[41] K.B. Zhanga, Z.Y. Fua, J.Y. Zhanga, J. Shi, W.M. Wanga, H. Wanga, Y.C. Wanga, Q.J. Zhang, Nanocrystalline CoCrFeNiCuAl high-entropy solid solution synthesized by mechanical alloying, J. Alloys Compd. 485 (2009) L31–L34.
[42] K.B. Zhang, Z.Y. Fu, J.Y. Zhang, W.M. Wang, S.W. Lee, K. Niihara, Characterization of nanocrystalline CoCrFeNiTiAl high-entropy solid solution processed by mechanical alloying, J. Alloys Compd. 459 (2010) 33–38.
[43] W. Ji, Z. Fu, W. Wang, H. Wang, J. Zhang, Y. Wang, F. Zhang, Mechanical alloying synthesis and spark plasma sintering consolidation of CoCrFeNiAl high-entropy alloy, J. Alloys Compd. 589 (2014) 61–66.
[44] O.A. Shcheretsky, High-entropy alloys, structure formation and crystallization, Metall. Met. Process. 1 (2013) 15–20.
[45] A.K. Singh, K. Kumar, A. Dwivedi, A. Subramaniam, A. Subramaniam, A geometrical parameter for the formation of disordered solid solutions in multi-component alloys, Intermetallics 53 (2014) 112–119.
[46] G.A. Salishchev, M.A. Tikhonovsky, D.G. Shaysultanov, N.D. Stepanov, A.V. Kuznetsov, I.V. Kolodiy, A.S. Tortika, O.N. Senkov, Effect of Mn and V on structure and mechanical properties of high-entropy alloys based on CoCrFeNi system, J. Alloys Compd. 591 (2014) 11–21.
[47] A. Munitz, M.J. Kaufman, M. Nahmany, N. Derimow, R. Abbaschian, Microstructure and mechanical properties of heat treated Al1.25CoCrCuFeNi high entropy alloys, Mater. Sci. Eng. A 714 (2018) 146–159.
[48] I. Moravcik, L. Gouvea, J. Cupera, I. Dlouhy, Preparation and properties of medium entropy CoCrNi/boride metal matrix composite, J. Alloys Compd. 748 (2018) 979–988.
[49] B.H. Gludovatz, A. Thurston, K.V. Bei, H. Wu, Z. George, E.P. Ritchie, RO., Exceptional damage-tolerance of a medium-entropy alloy CrCoNi at cryogenic temperatures, Nat. Commun. 7 (2016).
[50] Z. Wu, H. Bei, G.M. Pharr, E.P. George, Temperature dependence of the mechanical properties of equiatomic solid solution alloys with face-centered cubic crystal structures, Acta Mater. 81 (2014) 428–441.
[51] N. Chawla, Y.L. Shen, Mechanical behavior of particle reinforced metal matrix composites, Adv. Eng. Mater. 3 (6) (2001) 357–370.
[52] C. Wang, W. Ji, Z. Fu, Mechanical alloying and spark plasma sintering of $CoCrFeNiMnAl_5$ high-entropy alloy, Adv. Powder Technol. 589 (2014) 61–66.
[53] K.B. Zhang, Z.Y. Fu, J.Y. Zhang, W.M. Wang, H. Wang, Y.C. Wang, Q.J. Zhang, J. Shi, Microstructure and mechanical properties of CoCrFeNiTiAlx high-entropy alloys, Mater. Sci. Eng. A 508 (2009) 214–219.
[54] O.N. Senkov, J.M. Scott, S.V. Senkova, F. Meisenkothen, D.B. Miracle, C.F. Woodward, Microstructure and elevated temperature properties of a refractory TaNbHfZrTi alloy, J. Mater. Sci. 47 (9) (2012) 4062–4074.
[55] Inconel Alloy 718, http://www.specialmetals.com/documents/Inconelalloy718.pdf.
[56] Metals Handbook: V. 1: Properties and Selection: Irons, Steels and High-Performance Alloys.
[57] O.N. Senkov, G.B. Wilks, J.M. Scott, D.B. Miracle, Mechanical properties of Nb25Mo25Ta25W25 and V20Nb20Mo20Ta20W20 refractory high entropy alloys, Intermetallics 19 (2011) 698–706.
[58] O.N. Senkov, J.M. Scott, S.V. Senkova, D.B. Miracle, C.F. Woodward, Microstructure and room temperature properties of a high-entropy TaNbHfZrTi alloy, J. Alloys Compd. 509 (2011) 6043–6048.
[59] G.E. Dieter, Mechanical Metallurgy, third ed., McGraw-Hill, Inc., New York, 1986.
[60] H.J. McQueen, J.J. Jonas, in: Arsenault (Ed.), Treatise on Materials Science and Technology, Plastic Deformation of Materials, vol. 6, Academic Press, New York, 1975, pp. 393–493.